Gold and Gold−Iron Oxide Magnetic Glyconanoparticles: Synthesis, Characterization and Magnetic Properties.

Jesús M. de la Fuente,[†] David Alcántara,[†] Peter Eaton,[†] Patricia Crespo,[‡] Teresa C. Rojas,[§] Asunción Fernández,[§] Antonio Hernando,[‡] and Soledad Penadés*,[†]

Grupo de Carbohidratos, Laboratory of Glyconanotechnology, IIQ-CSIC, Américo Vespucio 49, 41092 Sevilla, Spain, Instituto de Magnetismo Aplicado, RENFE-UCM-CSIC and Departamento de Física de Materiales UCM, P.O. Box 155, Las Rozas, Madrid 28230, Spain, and Instituto de Ciencia de Materiales CSIC-UNSE, Américo Vespucio 49, 41092 Sevilla, Spain

Received: April 25, 2006; In Final Form: May 11, 2006

The preparation, characterization and the magnetic properties of gold and gold−iron oxide glyconanoparticles (GNPs) are described. Glyconanoparticles were prepared in a single step procedure in the presence of aqueous solution of thiol functionalized neoglycoconjugates and either gold salts or both gold and iron salts. Neoglycoconjugates of lactose and maltose disaccharides with different linkers were used. Iron-free gold or gold−iron oxide GNPs with controlled gold−iron ratios were obtained. The average core-size diameters are in the range of 1.5−2.5 nm. The GNPs are fully characterized by ^{1}H NMR spectrometry, transmission electron microscopy (TEM), and UV−vis and X-ray absorption (XAS) spectroscopies. Inductive plasma-atomic emission spectrometry (ICP) and elemental analysis gave the average number of neoglycoconjugates per cluster. The magnetic properties were measured in a SQUID magnetometer. The most remarkable results was the observation of a permanent magnetism up to room temperature in the iron-free gold GNPs, that was not present in the corresponding gold−iron oxide GNPs.

Introduction

The application of methodologies to produce nanoparticles with bioresponsive properties has opened the way for producing useful tools for molecular diagnostics, therapeutics, and biotechnology.[1−6] Metal, semiconductor, and magnetic colloidal nanoparticles are presently under intensive study for potential applications. The development of functional nanobioconjugates is mainly based on proteins and nucleic acids. However, carbohydrates as biologically important molecules have not received as much attention as protein- and gene-oriented nanotechnology.

We recently prepared, in a single step, sugar-protected gold nanoclusters. These tools are gold glyconanoparticles (GNPs) incorporating carbohydrate antigens for studying carbohydrate-mediated interactions.[7−9] The dispersion of these glyconanoparticles are stable for months in physiological solutions, and they have been shown to be excellent platforms for basic studies of carbohydrate interactions[10,11] and potential tools for biotechnological and biomedical applications.[12] In addition, they have an exceptionally small core size, which confers on them singular physical properties as materials (due to quantum confinement effects).

In an attempt to confer magnetism to these biofunctional gold nanoparticles and obtain new contrast agents based on stable nanoparticles protected with carbohydrates, we prepared gold−iron oxide glyconanoparticles by modification of the procedure used for preparation of the gold glyconanoparticles[8] and studied the magnetic behavior of AuFe GNPs. For the sake of comparison, pure Au GNPs were also measured.

Synthesis of magnetic nanoparticles with size control and suitably coated with polymers or other coating material to be dispersed into water is of interest for cell labeling and separation and for magnetic resonance imaging.[13−17] Commercially available iron oxide particles have been used in cell sorting and separation.[18] Magnetic nanoparticles coated with cross-linked dextran and functionalized with peptides and oligonucleotides have been prepared for intracellular labeling[19,20] and as nanosensors.[21] Biofunctional small (SPIO) and ultra-small (USPIO) iron oxide nanoparticles have been also prepared and used as a contrast agent in cellular labeling.[20] However, synthesis of magnetic particles with the desired size that are highly stable in aqueous solution without undergoing aggregation after some time and able to target a determined tissue or organ constitutes, even today, a problem to be solved. Surfactant-protected gold−iron core−shell nanoparticles have been recently synthesized by means of reverse micelles.[22] Attachment of biologically active molecules to this type of nanoclusters has, however, not been described.

We now report on a straightforward synthesis in aqueous solution of exceptionally small gold−iron oxide magnetic glyconanoparticles (AuFe−GNPs), which form stable colloidal solutions in water (ferrofluids) and present the study of their properties in comparison to those of the pure gold glyconanoparticles (Au−GNPs) previously prepared in our laboratory.[8] The singular (magnetic) properties found in both pure gold and gold−iron GNPs are also described.

Experimental Section

General Methods. All commercially available chemicals were used without further purification. Hydrogen tetrachloro-

* To whom correspondence should be addressed. E-mail: penades@iiq.csic.es.
[†] Laboratory of Glyconanotechnology.
[‡] Instituto de Magnetismo Aplicado.
[§] Instituto de Ciencia de Materiales.

10.1021/jp062522s CCC: $33.50
Published on Web 06/09/2006

aurate tetrahydrate, sodium tetrahydroborate, iron trichloride, lactose, and maltose were obtained from Aldrich. UV spectra were obtained by a UV/vis Perkin-Elmer Lambda 12 spectrophotometer. ^{1}H NMR spectra were acquired on a Bruker DRX-500 or DRX-300 spectrometer, and chemical shifts are given in ppm (δ) relative to D_2O. TEM examination of the samples was carried out at 200 keV with a Philips CM200 microscope. For the TEM characterization, a 10 μL drop of the aqueous solutions (0.1 mg/mL) of the glyconanoparticles was placed onto a copper grid coated with a carbon film. The grid was left to dry in air for several hours at room temperature. Particle size distributions of the nanoclusters were evaluated from several micrographs using an automatic image analyzer. EDX analysis was performed with a Philips DX4 spectrometer attached to the microscope. Elemental analysis was carried out in a LECO CHNS-932 apparatus after drying analytical samples under vacuum for 24 h. ICP analysis was performed in an Iris Advantage apparatus (Termo Jarrell Ash, Franklin, MA)

AFM measurements were made with a Topometrix explorer AFM (Veeco Instruments, Sunnyvale) in noncontact mode in air. The noncontact mode was used to avoid any compression of the sample that may have occurred with contact mode AFM. Rectangular silicon cantilevers with integrated tips of spring constant 4.5 N/m (MikroMasch, Tallinn, Estonia) were used, oscillating at just below their natural resonant frequency (normally 150 kHz but measured for each cantilever) throughout the work. Untreated glyconanoparticles were prepared for imaging by dissolving in pure water (18 MΩ, Sigma-Aldrich, U.K.). Glyconanoparticles were deposited onto freshly cleaved mica from dilute (70 μL·mL^{-1}) solution (5 μL per sample) and left to air-dry.

The magnetization measurements were done in a SQUID magnetometer (Quantum Design MPMS 5). The powder samples were fixed to the sample holder by means of a Kapton tape. Due to the low magnetization of the sample, an accurate determination of the magnetization was performed by measuring the sample holder and the Kapton tape used in each measurement. The magnetic signal (a diamagnetic one) arising from both, the sample holder and the Kapton tape, was then subtracted from the signal obtained once the sample was fixed and measured.

X-ray absorption spectra (XAS) for capped AuFe GNPs were recorded at room temperature in transmission mode at the beam line BM29 in the ESRF storage ring in samples supported on cellulose filters. Spectra were recorded at the Au L_3 edge at ca. 11 920 eV and the Fe K edge at ca. 7120 eV. To compare the XANES region of the XAS spectra, a linear background was fitted in the pre-edge region and subtracted before normalization to the edge jump.

Preparation of Neoglycoconjugates. Synthesis of lactose and maltose neoglycoconjugates **1** and **2** was carried out as previously described[8] by glycosidation of the conveniently protected sugar derivatives with 11-acetylthio-3,6,9-trioxaundecanol and 11-acetylthio-undecanol, respectively.

Preparation of Lactose Gold−Iron Oxide Glyconanoparticles *Lacto*(1-AuFe). To a solution of the disulfide **1** (140 mg, 0.14 mmol, 5.5 equiv) in MeOH (12 mL) a solution of $FeCl_3$ (2 mg, 0.013 mmol, 0.25 equiv) in water (0.5 mL) was added followed by addition of a solution of $HAuCl_4$ (17 mg, 0.05 mmol, 1 equiv) in water (2 mL). The mixture was left 5 min at room temperature, and then an aqueous solution of $NaBH_4$ (1 M, 52 mg, 1.38 mmol, 27.5 equiv) was added in small portions (250 μL) with rapid stirring. The brown suspension formed was stirred for an additional 2 h, and the solvent was removed under vacuum. The brown residue was dispersed in NANOpure water (~15 mL), loaded into a centrifugal filter device (CENTRIPLUS YM30, MICROCON, MWCO = 30 000), and subjected to centrifugation (3000*g*, 40 min). The dark glyconanoparticle residue was first washed with MeOH (5 mL) and then with water several times (8 × 5 mL) until the excess amount of neoglycoconjugate could no longer be detected by thin-layer chromatography (TLC). The residue was dispersed in water and centrifuged to eliminate insoluble materials, mainly gold and iron oxide precipitates. The brownish-clear solution was lyophilized, and the *lacto*(**1-AuFe**) GNPs obtained were free of salts and starting material (absence of signals from disulfide and Na^+ ions in ^{1}H and ^{23}Na NMR spectroscopy). Average diameter and number of gold atoms: 2 nm, 314. ^{1}H NMR (500 MHz, D_2O): δ 4.49 (brd, 1H, H-1′), 4.40 (brs, 1H, H-1), 4.10−3.30 (m, 23H), 2.92 (m, 0.5H). UV (H_2O, 0.3 mg·mL^{-1}): λ 500 nm, broad band. ICP: 51% Au, 2.8% Fe. Average formula: $(C_{20}H_{37}O_{14}S)_{95}Au_{266}Fe_{48}$.

Preparation of Maltose Gold−Iron Oxide Glyconanoparticles *Malto*(2-AuFe). To a solution of the disulfide **2** (80 mg, 0.075 mmol, 3 equiv) in methanol (11.5 mL) a solution of $FeCl_3$ (2 mg, 0.013 mmol, 0.25 equiv) in water (0.5 mL) was added followed by addition of a solution of $HAuCl_4$ (17 mg, 0.05 mmol, 1 equiv) in water (2 mL). The mixture was left 5 min at room temperature, and then an aqueous solution of $NaBH_4$ (1 M, 52 mg, 1.38 mmol, 27.5 equiv) was added in small portions (250 μL) with rapid stirring. The brown suspension formed was stirred for an additional 2 h, and the solvent was removed under vacuum. The brown residue was dispersed in NANOpure water (~15 mL), loaded into a centrifugal filter device (CENTRIPLUS YM30, MICROCON, MWCO = 30 000), and subjected to centrifugation (3000*g*, 40 min). The dark glyconanoparticle residue was first washed with MeOH (5 mL) and then with water several times (8 × 5 mL) until the excess amount of neoglycoconjugate could no longer be detected by thin-layer chromatography (TLC). The residue was dispersed in water and centrifuged to eliminate insoluble materials, mainly gold and iron oxide precipitates. The brownish-clear solution was lyophilized, and the *malto*(**2-AuFe**) GNPs obtained were free of salts and starting material (absence of signals from disulfide and Na^+ ions in ^{1}H and ^{23}Na NMR spectroscopy). Average diameter and number of gold atoms: 1.6 and 2.5 nm, 140 and 586. ^{1}H NMR (500 MHz, D_2O): δ 5.32 (s, 1H, H-1′), 4.37 (s, 1H, H-1), 4.00−3.30 (m, 13H), 2.70 (s, 2H, CH_2S), 1.85−1.20 (m, 17H). UV (H_2O, 0.3 mg·mL^{-1}): λ 500 nm, broad band. ICP: 28% Au, 0.27% Fe.

Preparation of Maltose Gold−Iron Oxide Glyconanoparticles *Malto*(2a-AuFe and 2b-AuFe). To a solution of the disulfide **2** (100 mg, 0.094 mmol, 3 equiv) in methanol (14 mL) a solution of $FeCl_3$ (2.5 mg, 0.01 mmol, 0.25 equiv) in water (0.63 mL) was added followed by addition of a solution of $HAuCl_4$ (21 mg, 0.04 mmol, 1 equiv) in water (2.5 mL). The mixture was left 5 min at 60 °C, and then an aqueous solution of $NaBH_4$ (1 M, 65 mg, 1.7 mmol, 27.5 equiv) was added in small portions with rapid stirring. The brown suspension formed was stirred for an additional 2 h. The crude product was separated by decantation from the methanolic solution. The brown residue was dispersed in NANOpure water (~15 mL), loaded into a centrifugal filter device (CENTRIPLUS YM30, MICROCON, MWCO = 30 000), and subjected to centrifugation (3000*g*, 40 min). The dark glyconanoparticle residue was first washed with MeOH (5 mL) and then with water several times (8 × 5 mL) until the excess amount of neoglycoconjugate could no longer be detected by thin-layer chromatography

SCHEME 1

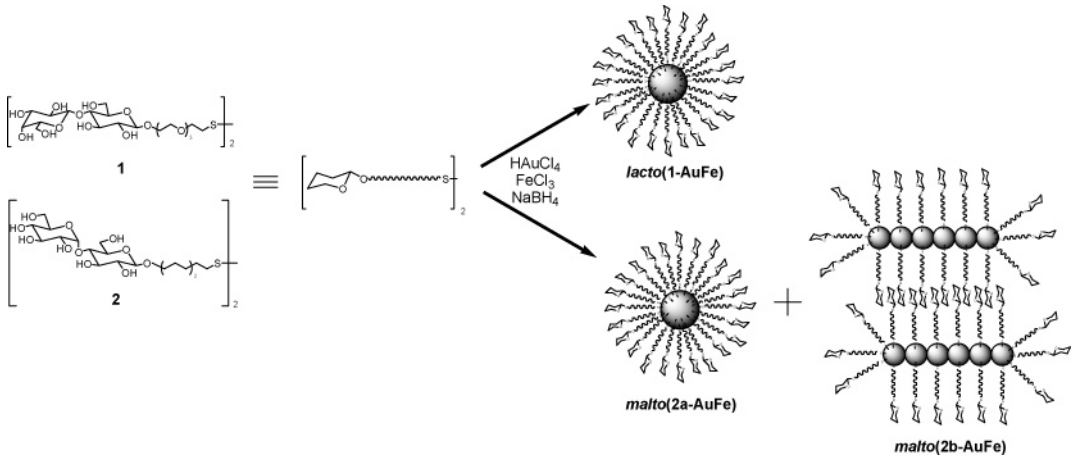

(TLC). The residue was dispersed in water and centrifuged to eliminate insoluble materials, mainly gold and iron oxide precipitates. The brownish-clear solution was lyophilized, and the *malto*(**2a-AuFe**) GNPs obtained were free of salts and starting material (absence of signals from disulfide and Na^+ ions in ^1H and ^{23}Na NMR spectroscopy). Average diameter and number of gold atoms: 1.8 nm, 201. ^1H NMR (500 MHz, D_2O): δ 5.32 (s, 1H, H-1′), 4.37 (s, 1H, H-1), 4.00−3.30 (m, 13H), 2.70 (s, 2H, CH_2S), 1.85−1.20 (m, 17H). UV (H_2O, 0.3 mg·mL^{-1}): λ 500 nm, broad band. ICP: 23.7% Au, 0.346% Fe. Anal. Calcd for $(C_{23}H_{44}O_{11}S)_{191}Au_{191}Fe_{10}$: C, 37.9; H, 5.9; S, 4.4. Found: C, 34.2; H, 5.5; S, 4.0.

The colorless methanolic dispersion obtained from the crude reaction product was evaporated, and a white residue was isolated. The residue was dispersed in water and centrifugal filtered (CENTRIPLUS YM30, MICROCON, MWCO = 30 000, 3000*g*, 40 min) and washed with water (8 × 5 mL). The residue was dissolved in water and lyophilized to give *malto*(**2b-AuFe**) as a white solid. Average diameter and number of gold atoms: 1.5 nm, 79. ^1H NMR (500 MHz, D_2O): δ 5.32 (s, 1H, H-1′), 4.37 (s, 1H, H-1), 4.00−3.30 (m, 13H), 2.70 (s, 2H, CH_2S), 1.85−1.20 (m, 17H). UV (H_2O, 2 mg·mL^{-1}): λ 500 nm, broad band. ICP: 0.815% Au, 0.039% Fe. Anal Calcd for $(C_{23}H_{44}O_{11}S)_{2050}Au_{67}Fe_{12}$: C, 51.7; H, 8.1; S. 6.0. Found: C, 50.6; H, 7.9; S, 5.8.

Preparation of Lactose and Maltose Gold Glyconanoparticles *Lacto*(1-Au) and *Malto*(2-Au). The iron-free *lacto*(**1**-Au) and *malto*(**2-Au**) GNPs were prepared as previously described[8] but avoiding the use of Fe-contaminating material. ICP analysis confirmed that the iron content of these GNPs is below 0.01 ppm.

Results and Discussion

The procedure now reported for the synthesis of AuFe−GNPs is similar to that used for the synthesis of pure Au−GNPs by which neoglycoconjugates of significant carbohydrates are covalently linked to gold/iron oxide clusters as a method for tailoring stable, magnetic glyconanoparticles with globular shapes and highly polyvalent carbohydrate surfaces. The methodology also allows attachment of many other molecules directly to the nanocluster, as already reported for the preparation of gold glyconanoparticles.[8] In our approach formation of the gold and gold−iron oxide (AuFe) cluster and linking of the carbohydrate antigen to the gold is a simultaneous process, so that the presence of the neoglycoconjugate controls the shape and size of the nanoclusters. This approach opens the way for tailoring glyconanoparticles with a variety of carbohydrate ligands and very useful magnetic properties for future applications as ferrofluids in molecular imaging and tumor targeting.[23] The so-prepared glyconanoparticles have less than a 2 nm diameter core. They formed stable dispersions, and even after several months, flocculation or aggregation was not observed.

Thiol-functionalized neoglycoconjugates of the disaccharides lactose (*lacto*, Galβ1−4Glcβ1-OR) and maltose (*malto*, Glcα1−4Glcβ1-OR) have been synthesized to prepare the magnetic nanoparticles in situ (Scheme 1). The disaccharides lactose and maltose were chosen to compare the gold−iron oxide with the pure gold *lacto*(**1-Au**) and *malto*(**2-Au**) GNPs previously prepared.[8] The synthesis of lactose and maltose neoglycoconjugates **1** and **2** was carried out as previously described by glycosydation of the conveniently protected sugar derivatives with 11-acetylthio-3,6,9-trioxa-undecanol and 11-acetylthio-undecanol, respectively.[8] Different linkers have been used to test the influence of their hydrophilic or hydrophobic nature in the properties of the whole material. Neoglycoconjugates **1** and **2** were isolated as disulfide forms and used in this form for the preparation of AuFe-protected glyconanoparticles. A water/methanol solution of $FeCl_3$ and $HAuCl_4$ in a ratio of 1:4 was reduced with $NaBH_4$ in the presence of disulfides **1** and **2** to give stable dispersions of *lacto*(**1-AuFe**), and *malto*(**2a-AuFe**), and *malto*(**2b-AuFe**) GNPs in a single step. Pure gold *lacto*(**1-Au**) and *malto*(**2-Au**) GNPs (Fe content below 0.01 ppm) were also prepared, and special care was taken to avoid contamination by iron-containing materials.

The ^1H NMR in deuterated water, TEM micrographs, and the corresponding particle size distribution histograms for the AuFe GNPs are shown in Figure 1. The corresponding data for the Au GNPs were already described.[8] For the lactose glyconanoparticles, *lacto*(**1-AuFe**), the corresponding histogram gives a mean diameter for the gold−iron oxide cluster of 2 nm, which corresponds to an average number of 314 atoms (Figure 1a).[24] In the case of *malto*(**2-AuFe**) two different fractions could be obtained depending on the isolation procedure (see Experimental Section). In the first procedure a mixture of two different nanostructures could be observed on the micrographs: dispersed nanoclusters and areas with linearly ordered nanoparticles (Figure 1c). The corresponding histogram gave a bimodal particle size distribution centered at 1.6 and 2.5 nm. The two types of nanostructures could be isolated separately following the second procedure. A methanol-insoluble brown residue was isolated which corresponds to *malto*(**2a-AuFe**) GNPs. The micrographs have a particle size distribution centered at 1.8 nm,

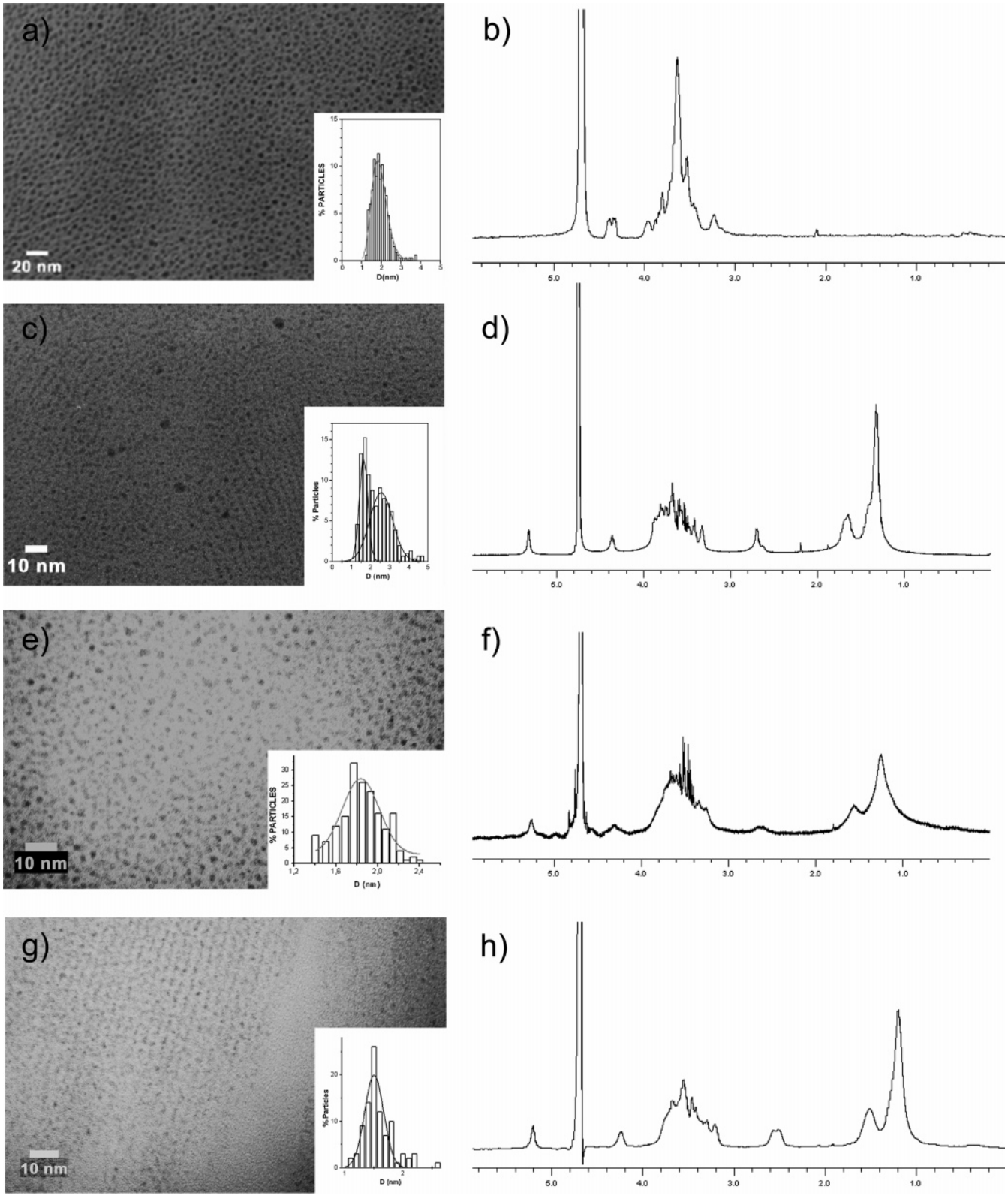

Figure 1. Transmission electron micrographs and ^{1}H NMR spectra of (a and b) *lacto*(**1-AuFe**), (c and d) *malto*(**2-AuFe**), (e and f) *malto*(**2a-AuFe**), and (g and h) *malto*(**2b-AuFe**). The corresponding particle size distribution histograms of the protected nanoparticles are also included.

as indicated by the corresponding histogram (Figure 1e). From the methanol solution a white residue was obtained that was not detected in the methanol solution of the *lacto*(**1-AuFe**). The isolated white solid, *malto*(**2b-AuFe**), also formed water-stable dispersions and contains very small AuFe nanoparticles perfectly aligned and encapsulated in what seems to be organic material as indicated by the TEM micrographs. The corresponding histogram gave a particle size distribution of less that 1.5 nm diameter, and the distance between the ordered lines is around 3.4 nm (Figure 1g). Elemental analysis of *malto*(**2b-AuFe**) indicates that more than 2000 maltose molecules surrounded the AuFe cluster. The amphiphilic character of the maltose neoglycoconjugate **2** (with a lipophilic spacer C11) may be the origin of these supramolecular aggregates in water solution.

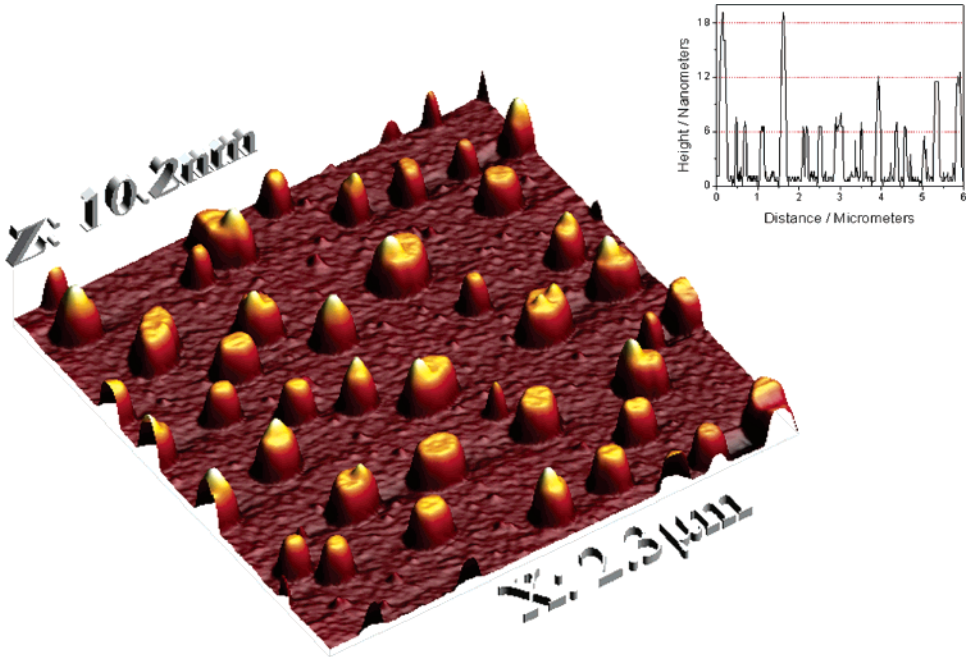

Figure 2. Typical AFM image of sample *malto*(**2b-AuFe**). (Inset) Line scan through a larger image of sample with horizontal lines at $z = 6$, 12, and 18 nm for guidance.

Neoglycolipids such as *n*-dodecyl β-maltoside,[25] *n*-octyl β-glucoside, and phenyl-alkyl β-glucosides are known to form micelles and other types of aggregates.[26] Encapsulation of Au nanocrystals in a nanotube formed by a β-glucolipid has been recently described.[27] Capsules were not observed for *lacto*(**1-AuFe**). Neoglycoconjugate **1** has the much less lipophilic linker tetra(ethylene glycol) and therefore is not expected to behave in an amphiphilic manner.

Elemental and inductive coupled plasma-atomic emission spectrometry (ICP) gave an average composition of 95 lactose molecules, 266 gold atoms, and 48 iron atoms for *lacto*(**1-AuFe)**, 190 maltose molecules, 190 gold atoms, and 10 iron atoms for *malto*(**2a-AuFe)**, and 2050 maltose molecules, 67 gold atoms, and 10 iron atoms for *malto*(**2b-AuFe**), which corresponds to an average Au:Fe ratio of 5:1, 20:1, and 6:1, respectively. In the case of *malto*(**2b-AuFe)** the 2000 maltose molecules in excess accounts for formation of the organic nanocapsules.

Atomic force microscopy (AFM) images confirm this encapsulation (Figure 2). These images strongly differ from those usually obtained for isolated *lacto*(**1-Au**) and *malto*(**2-Au**) glyconanoparticles.[28] In addition to small particles of mean height 1.3 nm, broad flat aggregates of around 6, 12, or 18 nm height were observed which correspond to the distance of two, four, or six consecutive maltose neoglycoconjugates **2**, indicating that growth of these aggregates is controlled by the maltose neoglycoconjugate. These results, along with the elemental analysis, suggest the presence of two components in the sample: the organic neoglycoconjugate aggregates and the nanoparticles with a metal core.

The UV/vis spectra of these GNPs show weak surface plasmon absorption around 500 nm. The absorption bands of *lacto*(**1-AuFe**) and *malto*(**2a-AuFe**) (Figure 3a and 3b) strongly decrease in comparison with the absorption spectrum of 10 nm gold nanoclusters. This is probably due to the very small dimension of the nanoclusters (below 2 nm).[29] However, it is worth highlighting that the surface plasmon band of *malto*(**2b-AuFe**) increases (Figure 3c), probably due to the short distance between the metallic glyconanoparticles along the lines (Figure 1g).

Figure 4 shows the XANES spectra of the Au L_3-edge and the Fe K-edge for *lacto*(**1-AuFe**) and *malto*(**2-AuFe**). The XANES region of the XAS spectra contains information about oxidation states and local structure around the absorbing atom, and it can also be used like a fingerprint technique to obtain results only by comparison with references samples. A threshold resonance at the Au L_3 absorption that is just below the one for the bulk gold was observed (Figure 4a). In the case with particles 2 nm in diameter, the lattice contraction effect was almost totally compensated by the charge transfer to the capping molecules. This effect was also observed in the case of *malto*(**2-Au)** samples.[30] Figure 4b shows the spectra at the Fe K edge for the *lacto*(**1-AuFe**) and *malto*(**2-AuFe**) samples together with the spectra measured for a metallic Fe foil, γ-Fe_2O_3, and Fe_3O_4 references. It is clear that the spectra of the samples are similar to the oxide ones, and furthermore, the intensity of the features at 7113 eV and of the white line at 7132 eV seems to indicate that the Fe atoms contained in the sample are more similar to the Fe_3O_4 structure.

High-resolution TEM was performed to better characterize the structure of the inorganic core. However, after several trials we were not able to obtain high-resolution micrographs of these samples, probably due to the small size of the nanoparticles and the large amount of organic material covering and protecting the inorganic cores, making these measurements extremely difficult. Nevertheless, due to the low amount of iron oxide included in the inorganic cores (2.8−0.04% Fe) it is improbable to have a core−shell structure. Iron must be dissolved into the gold phase.

Magnetic characterization of the gold and gold−iron GNPs reveals singular properties in these nanoclusters. Magnetization curves as a function of the applied field at different temperatures as well as the dependence of magnetization with the temperature have been measured for the gold−iron oxide and iron-free gold GNPs. It was very remarkable to observe a ferromagnetic-like behavior not only for the AuFe GNPs but also for the pure gold GNPs (Figure 5). In the AuFe samples a ferromagnetic behavior

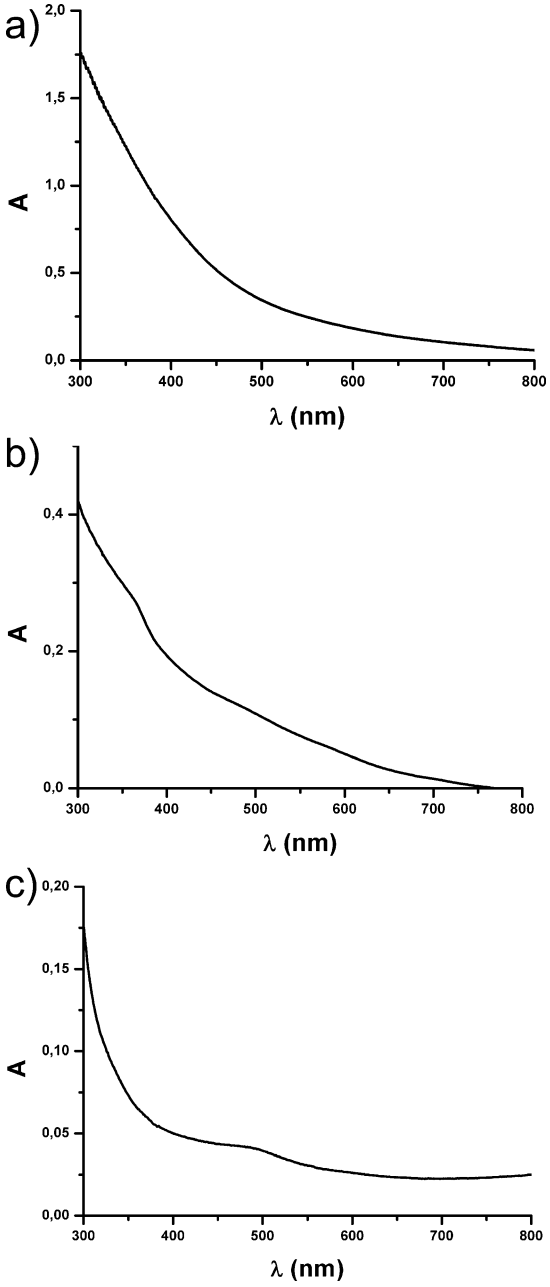

Figure 3. UV absorption spectra of (a) *lacto*(**1-AuFe**), (b) *malto*(**2a-AuFe**), and (c) *malto*(**2b-AuFe**).

at 5 K with small hysteresis cycle was observed (Figure 5a, 5c, and 5e). The coercive field values at 5 K were around 15, 45, and 80 Oe for *lacto*(**1-AuFe**), *malto*(**2a-AuFe**), and *malto*(**2b-AuFe**), respectively. The samples were far from being saturated, with magnetization values at 1 T of around 0.125 (0.24 emu/g AuFe), 0.044 (0.16 emu/g AuFe), and 0.008 emu/g (0.64 emu/g AuFe) for *lacto*(**1-AuFe**), *malto*(**2a-AuFe**), and *malto*(**2b-AuFe**), respectively. These values were obtained after subtracting the diamagnetic contribution of the sample holder (Kapton). As shown in Figure 5f, both the measurements of the Kapton tape and the Kapton plus the sample are completely different. In the case of the *malto*(**2b-AuFe**) sample, the diamagnetic contribution associated with the organic component has been subtracted for determining the magnetization of the nanoparticles. Although the Fe content determined in the samples (3.0%, 0.4%, and 0.04% for *lacto*(**1-AuFe**), *malto*(**2a-AuFe**), and *malto*(**2b-AuFe**), respectively) would account for the magnetization values, it is difficult to attribute the magnetic hysteresis

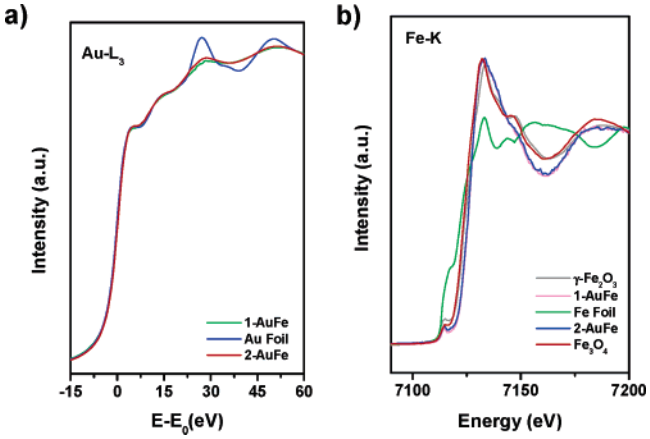

Figure 4. (a) Au L_3-XANES spectra for *lacto*(**1-AuFe**) and *malto*(**2-AuFe**) compared to bulk gold (Au foil), and (b) Fe K-XANES spectra for *lacto*(**1-AuFe**) and *malto*(**2-AuFe**) compared to Fe foil, γ-Fe_2O_3, and Fe_3O_4 references.

observed to the presence of iron, in particular to Fe_3O_4. For instance, the blocking temperature of 5 nm Fe_3O_4 particles is around 45 K.[31] From this value, and assuming spherical particles, it can be estimated that 2 nm pure Fe_3O_4 nanoparticles would exhibit a blocking temperature of around 3 K. Taking into account that in our case Fe_3O_4 is the minor component of the nanoparticles, a blocking temperature lower than 3 K should be expected. As can be seen in Figure 5, all AuFe GNPs exhibit hysteresis at 5 K and, in particular, the one with the lower Fe content (*malto*(**2b-AuFe**)) exhibits hysteresis at 300 K.

Even more unexpected was the ferromagnetic behavior observed for the iron-free *lacto*(**1-Au**) and *malto*(**2a-Au**) GNPs with coercive field values of 100 and 125 Oe higher than those observed for the AuFe GNPs (Figure 5b and 5d). By increasing the temperature the magnetic hysteresis in *lacto*(**1-AuFe**) and *malto*(**2a-AuFe**) GNPs disappears and a paramagnetic behavior is observed, whereas a ferromagnetic component remains even at room temperature for *malto*(**2b-AuFe**) (Figure 5e). This result is quite unexpected since, as mentioned previously, the Fe content in *lacto*(**1**-AuFe) GNPs is much higher than that in *malto*(**2a-AuFe**), suggesting that the origin of the magnetic properties of the systems cannot be merely attributed to the presence of iron oxide. Moreover, the average size of *malto*(**2a-AuFe**) nanoparticles is smaller than that of the *lacto*(**1-AuFe**) nanoparticles; therefore a "weak" ferromagnetic behavior could be expected. In addition, if the magnetization is referred to the weight fraction of gold atoms which are bonded to the thiol group, instead of to the total amount of sample, the magnetization values obtained become similar and around 0.1 emu/g Au bonded for both set of samples, suggesting that this ferromagnetic behavior can be attributed to the Au content instead of to the Fe content. This is confirmed by the magnetic hysteresis observed even at room temperature in the iron-free *lacto*(**1-Au**) and *malto*(**2-Au**) GNPs (Figure 5b and 5d). Observation of a permanent magnetism in the pure gold GNPs was so unexpected (mannose and other sugar thiol-capped GNPs present also this magnetism) that the magnetic properties of thiol-functionalized gold nanoparticles were compared with detergent-protected gold nanoparticles. Gold nanoparticles with commercially available 1-dodecanethiol and an average size of 1.5 nm were prepared. The results confirmed that a ferromagnetic behavior was also presented even up to room temperature only for the thiol-protected Au nanoparticles.[32] We proposed two factors to be in the origin of the ferromagnetic-like behavior: the small particle size (below 2 nm) and the change on the

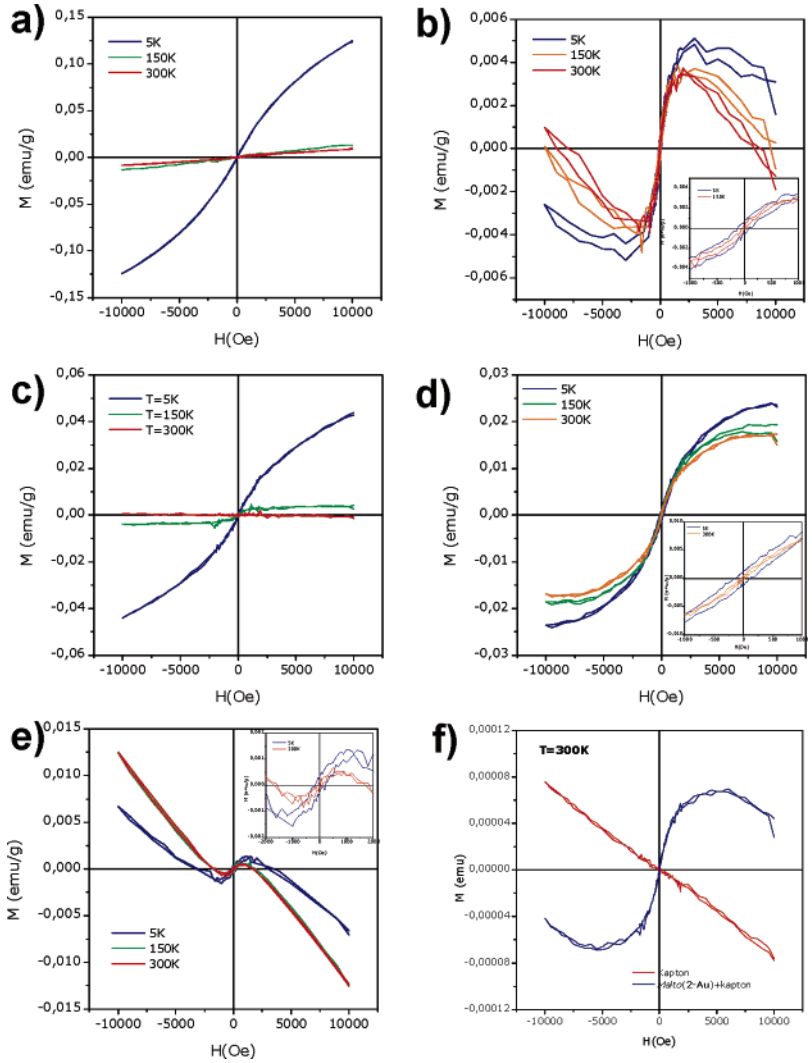

Figure 5. Magnetization curves measured between 5 K and room temperature for (a) *lacto*(**1-AuFe**), (b) *lacto*(**1-Au**), (c) *malto*(**2a-AuFe**), (d) *malto*(**2-Au**), and (e) *malto*(**2b-AuFe**), and (f) an example of curves measured for the diamagnetic Kapton tape and the *malto*(**2-Au**) sample plus the Kapton tape. (Insets) Magnifications of the hysteresis loops.

electronic structure of the Au nanoparticle due to the covalent Au−thiol bond.[33] From XANES data it was inferred that this behavior is related with a strong charge transfer between the Au atom and the S atom, localized 5d holes generated through the Au−S bond. The d-charge loss has been estimated to be a maximum as 0.05 e/atom, a low value that is in agreement with the low values of the measured magnetization.[32] This effect seems to also be in the origin of the magnetic behavior observed in AuFe nanoparticles reported here. The fast decrease of the magnetization at low temperatures could be attributed to the small amount of Fe present in the nanoparticles in the *lacto*(**1-AuFe**) and *malto*(**2a-AuFe**) (Figure 5a and 5c). The hysteresis observed at low temperatures in the AuFe GNPs is more likely attributable to the surface Au atoms which are bonded to the thiol group.[34]

The origin of permanent magnetism in thiol-protected Au GNPs is still unclear, and many questions still remain. A more detailed study to understand the differences in the magnetic behavior of AuFe− and Au−GNPs is presently underway.

Conclusions

In conclusion, we developed a simple methodology to prepare exceptionally small, water-dispersible, and stable magnetic nanoparticles covalently linked to oligosaccharides. The methodology can be extended to the preparation of hybrid nanoparticles incorporating both carbohydrates and other molecules (fluorescence probes, biotin, etc.).[8] Carbohydrate−receptor interactions can direct the magnetic glyconanoparticles to target cells and tissues, allowing their selective labeling. This kind of polyvalent magnetic glyconanoparticles complements the already available bioactive iron oxide magnetic nanoparticles.[19−21,34] However, the most striking fact of these results is the singular observation of a permanent magnetism in the pure gold GNPs with coercive fields higher than those of the gold−iron oxide GNPs. The easy preparation and purification, their small core size and stability, and their dispersability in physiologically relevant conditions together with their exceptional magnetic properties make these particles potential candidates for diagnostic, tumor targeting,[23] or magnetic resonance imaging[34] applications. The response of different cellular lines against these magnetic glyconanoparticles and their longitudinal and transversal relaxation times, T_1 and T_2, in buffer and plasma are presently being determined.

Acknowledgment. XAS facilities at BM29 in ESRF and the technical support from O. Mathon are acknowledged. This research was supported by the Spanish Ministerio de Educación y Ciencia (NAN2004-09125-C07) and CSIC (PIF2005). J.M.F.,

P.E., and D.A. thank the Spanish Ministerio de Educacion y Ciencia (MEC) for financial support.

References and Notes

(1) Niemeyer, C. M. *Angew. Chem., Int. Ed.* **2001**, *40*, 4128.
(2) Katz, E.; Willner, I. *Angew. Chem., Int. Ed.* **2004**, *33*, 6042.
(3) Daniel, M.-C.; Astruc, D. *Chem. Rev.* **2004**, *104*, 293.
(4) Verma, A.; Rotello, V. M. *Chem. Commun.* **2005**, *3*, 303.
(5) Drechesler, U.; Erdogan, B.; Rotello, V. M. *Chem.*—Eur. J. **2004**, *10*, 5570.
(6) Wang, J. *Small* **2005**, *1*, 1036.
(7) de la Fuente, J. M.; Barrientos, A. G.; Rojas, T. C.; Rojo, J.; Cañada, J.; Fernández, A.; Penadés, S. *Angew. Chem., Int. Ed.* **2001**, *40*, 2257.
(8) Barrientos, A. G.; de la Fuente, J. M.; Rojas, T. C.; Fernández, A.; Penadés, S. *Chem.*—Eur. J. **2003**, *9*, 1909.
(9) Hernáiz, M. J.; de la Fuente, J. M.; Barrientos, A. G.; Penadés, S. *Angew. Chem., Int. Ed.* **2002**, *41*, 1554.
(10) de la Fuente, J. M.; Penadés, S. *BBA-Gen. Subjects* **2006**, *1760*, 636.
(11) de la Fuente, J. M.; Penadés, S. *Glycoconjugate J.* **2004**, *21*, 149.
(12) Rojo, J.; Díaz, V.; de la Fuente, J. M.; Segura, I.; Barrientos, A. G.; Riese, H.-H.; Bernad, A.; Penadés, S. *ChemBioChem* **2005**, *5*, 291.
(13) Huber, D. L. *Small* **2005**, *1*, 482.
(14) Tartaj, P.; Morales, M. P.; Veintemillas-Verdaguer, S.; Gonzalez-Carreño, T.; Serna C. J. *J. Phys. D: Appl. Phys.* **2003**, *36*, R182
(15) Mornet, S.; Vasseur, S.; Grasset, F.; Duguet, E. *J. Mater. Chem.* **2004**, *14*, 2161.
(16) Berry, C. C.; Curtis, A. S. G. *J. Phys. D: Appl. Phys.* **2003**, *36*, R198.
(17) Pankhurst, Q. A.; Connolly, J.; Jones, S. K.; Dobson, J. *J. Phys. D: Appl. Phys.* **2003**, *36*, R167.
(18) Whitesides, G. M.; Kazlauskas R. J.; Josephson L. *Trends Biotechnol.* **1983**, *1*, 144.
(19) Josephson, L.; Tung, C.-H.; Moore, A.; Weissleder, R. *Bioconjugate Chem.* **1999**, *10*, 186.
(20) Lewin, M.; Carlesso, N.; Tung, C.-H.; Tang, X.-W.; Cory, D.; Scadden, D. T.; Weissleder, R. *Nat. Biotechnol.* **2000**, *18*, 410.
(21) Josephson, L.; Pérez, J. M.; Weissleder, R. *Angew. Chem., Int. Ed.* **2001**, *40*, 3204.
(22) Zhou, W. L.; Carpenter, E. E.; Lin, J.; Kumbhar, A.; Sims, J.; O'Connor, C. J. *Eur. Phys. J. D* **2001**, *16*, 289.
(23) Mykhaylyk, O.; Cherchenko, A.; Ilkin, A.; Dudchenko, N.; Ruditsa, V.; Novoseletz, M.; Zozulya, Y. *J. Magn. Magn. Mater.* **2001**, *225*, 241.
(24) Hostetler, M. J.; Wingate, J. E.; Zhong, C.-J.; Harris, J. E.; Vachet, R. W.; Clark, M. R.; Londono, J. D.; Green, S. J.; Stokes, J. J.; Wignall, G. D.; Glish, G. L.; Porter, M. D.; Evans, N. D.; Murray, R. W. *Langmuir* **1998**, *14*, 17.
(25) Kuhlbrandt, W. *Q. Rev. Biophys.* **1988**, *21*, 429.
(26) Jung, J. H.; John, G.; Yoshida, K.; Shimizu, T. *J. Am. Chem. Soc.* **2002**, *124*, 10674.
(27) Yang, B.; Kamiya, S.; Yoshida, K.; Shimizu, T. *Chem. Commun.* **2004**, 500.
(28) de la Fuente, J. M.; Eaton, P.; Barrientos, A. G.; Menendez, M.; Penades, S. *J. Am. Chem. Soc.* **2005**, *127*, 6192.
(29) Murray, C. B.; Kagan, C. R.; Bawendi, M. G. *Annu. Rev. Mater. Sci.* **2000**, *30*, 545.
(30) López-Cartes, C.; Rojas, T. C.; Litrán, R.; Martínez-Martínez, D.; de la Fuente, J. M.; Penadés, S.; Fernández, A. *J. Phys. Chem. B* **2005**, *109*, 8761.
(31) Goya, G. F.; Berquó, T. S.; Fonseca, F. C.; Morales, M. P. *J. Appl. Phys.* **2005**, *95*, 3520.
(32) Crespo, P.; Litrán, R.; Rojas, T. C.; Multigner, M.; de la Fuente, J. M.; Sánchez-López, J. C.; García, M. A.; Hernando, A.; Penadés, S.; Fernández, A. *Phys. Rev. Lett.* **2004**, *93*, 087204.
(33) Hernando, A.; Crespo, P.; García, M. A. *Phys. Rev. Lett.* **2006**, *96*, 057206.
(34) Josephson, L.; Kircher M. F.; Mahmood, U.; Tang, Y.; Weissleder, R. *Bioconjugate Chem.* **2002**, *13*, 554.